Nonlinear Modeling and Investigating the Nonlinear Effects on Frequency Response of Silicon Bulk-Mode Ring Resonator

A. Bijari*, S. H. Keshmiri* and W. Wanburee**

Abstract: This paper presents a nonlinear analytical model for silicon micromechanical ring resonators with bulk-mode vibrations. A distributed element model has been developed to describe the dynamic behavior of the micromechanical ring resonator. This model shows the nonlinear effects in a silicon ring resonator focusing on the effect of large amplitudes around the resonance frequency, material and electrical nonlinearities. Through the combination of geometrical and material nonlinearities, closed-form expressions for third-order nonlinearity in mechanical stiffness of bulk-mode ring resonators are obtained. Using the perturbation method and the method of harmonic balance, the expressions for describing the effect of nonlinearities on the resonance frequency and stability are derived. The results, which show the effect of varying the AC-drive voltage, initial gap spacing, DC-bias voltage and the quality factor on the frequency response and resonant frequencies, are discussed in detail. The nonlinear model introduces an appropriate method in the field of bulk-mode ring resonator design for achieving sufficient power handling and low motional resistance.

Keywords: Micromechanical ring resonator, Nonlinearity, Bulk-mode, Frequency response, Power handling.

1 Introduction

Development of micromechanical resonators and filters with high quality factor, high power handling capability and low motional resistance, is currently one of the interesting subjects in micro-communication applications [1]. The silicon micromechanical resonators due to their small size, low cost and compatibility with integrated circuit (IC) technology are a promising alternative to surface acoustic wave (SAW) and quartz crystal resonators. However, low motional resistance and high power handling make them difficult to handle with linearity and small size. And, due to their small size, these resonators cannot store high energy and, therefore, they should be driven at high excitation value which causes them to be easily driven into nonlinear regimes [2]. Moreover, the most direct methods for lowering the motional resistance in micromechanical resonators, like scaling down the electrode to resonator gap and raising the DC-bias voltage, decrease the linearity [3]. The ability to accurately model nonlinearity and investigate its effect on frequency response is, therefore, a key requirement to optimum design of silicon micromechanical resonators. There are some mechanical and electrical nonlinearities in silicon micromechanical resonators. Depending on the resonator design and operating conditions, different nonlinearities may be dominant and result in hardening or softening behavior in the dynamic behavior of micromechanical resonator [4]. A lot of research has been conducted on modeling the nonlinear effects in micromechanical resonators. Gui *et al*. [5] investigated the nonlinear effects on the performance of a micro-bridge, using Rayleigh's energy method, and showed the dependency of the hysteresis criterion on the quality factor, operating conditions, geometric and material properties of the micromechanical resonator. Mestrom *et al*. [4] studied the frequency responses and the nonlinear dynamic properties of clamped-clamped beam resonator and predicted the hardening behavior. They also compared their analytical results with the results from experiments and found a reasonable agreement. Alastalo *et al*. [6] presented a very useful study on the longitudinal mode resonators with respect to mechanical and electrical nonlinearity. Assuming a high quality factor, some of

Iranian Journal of Electrical & Electronic Engineering, 2012.
Paper first received 10 Aug. 2011 and in revised form 23 Oct. 2011.
* The Authors are with the Department of Electrical Engineering, Faculty of Engineering, Ferdowsi University of Mashhad (FUM), 91775-1111, Iran.
E-mails: a.bijari@gmail.com and keshmiri@um.ac.ir.
** The Author is with the School of Electrical Engineering, Institute of Engineering, Suranaree University of Technology (SUT), Nakhon Ratchasima 30000, Thailand.
E-mail: Electrical.sut@gmail.com.

the aforementioned works have ignored damping coefficient in calculating the shift resonance frequency caused by nonlinearities. Moreover, the study on the nonlinearities in bulk-mode micromechanical resonators is inadequate, and previous works have only focused on the longitudinal and square extensional mode resonators [7]. This paper deals with the effects of nonlinearities on frequency response of silicon bulk-mode ring resonators. First, a comprehensive nonlinear model of the resonator is derived. The model includes the effect of large amplitudes around the resonance frequency, material and electrical nonlinearities. Then, the effect of key parameters on nonlinear frequency response is evaluated applying perturbation techniques and harmonic balance method. Finally, the validity of the model is verified by comparison with the experimental data obtained by Xie *et al*. [8] in linear regime, and two analytical models presented by Zhang *et al*. [9] and Kaajakari *et al*. [10], [11] in nonlinear regime.

2 Bulk-Mode Ring Resonator

Among silicon micromechanical resonators, bulk-mode ring resonators offer lower motional resistance and higher quality factor due to their high structural stiffness, ring geometry and having four quasi-nodal points at their outer periphery in some non-axisymmetric bulk-modes like wine glass and extensional wine glass. Therefore, they are more extensively developed in RF transceiver front-end architectures [8].

In the bulk-mode ring resonators which are shown in Fig. 1, assuming that the width of the ring is much larger than its thickness (R_o-R_i >> t), the 2-D linear equations governing the vibration of a ring, without body force and internal heat source can be given by [12], [13]:

$$\nabla\left(\frac{E\cdot A}{1-\upsilon^2}\nabla\cdot\mathbf{u}\right)-\frac{E\cdot A_0}{2(1+\upsilon)}\nabla\times\nabla\times\mathbf{u}=\rho A_0\frac{\partial^2\mathbf{u}}{\partial t^2} \quad (1)$$

where E, υ, ρ and A are Young's modulus, Poisson's ratio, density of structural material and transduction area of the resonator, respectively. The displacement vector $\mathbf{u}=x\mathbf{e_r}+w\mathbf{e_\theta}$ is defined in terms of the radial (x) and circumferential displacements (w) in polar coordinates through the time and mode shape functions as follows:

$$x(t,\theta)=X_r(t)\cdot\cos(n\theta),\ w(t,\theta)=W_r(t)\cdot\sin(n\theta) \quad (2)$$

where

$$X_r(t)=\sum_{q=1}^{\infty}X_{rq}\cos(q\omega t),\quad W_r(t)=\sum_{q=1}^{\infty}W_{rq}\cos(q\omega t) \quad (3)$$

where at the natural resonance frequency of $\omega_{nm}=h_{nm}\sqrt{(E/\rho(1-\upsilon^2)}$, the radial displacement at inner and outer radius can be assumed as:

$$x_o(t,\theta)=X_o(t)\cdot\cos(n\theta),\ x_i(t,\theta)=X_i(t)\cdot\cos(n\theta) \quad (4)$$

and approximately,

$$X_o(t)=U_o\cos(\omega t),\quad X_i(t)=U_i\cos(\omega t) \quad (5)$$

where, $U_o=U_{r=Ro}$ and $U_i=U_{r=Ri}$ can be expressed by following equation:

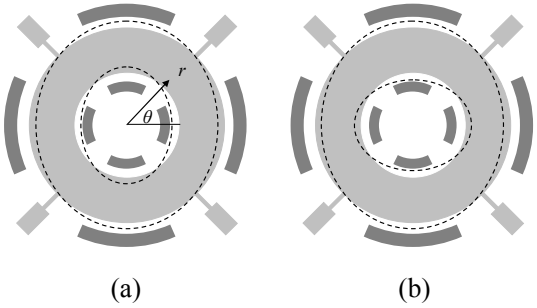

Fig. 1 The schematic views of the bulk-mode shapes of the ring resonator a) wine glass b) extensional wine glass.

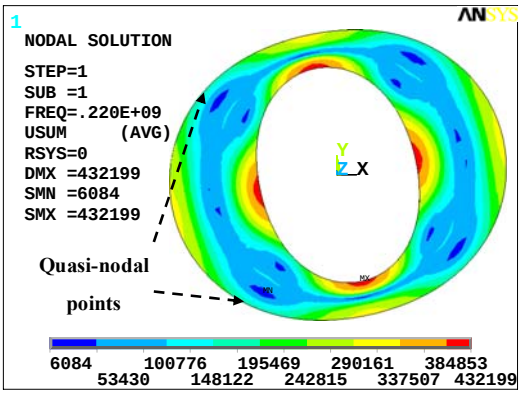

Fig. 2 ANSYS simulation of EWG mode shape ring resonator.

$$U_r=\frac{A_n}{h_{nm}}\left[\frac{d}{dr}\left(J_n(h_{nm}r)+\frac{B_n}{A_n}Y_n(h_{nm}r)\right)+\frac{n}{r}\left(\frac{C_n}{A_n}J_n(h_{nm}r)+\frac{D_n}{A_n}Y_n(h_{nm}r)\right)\right] \quad (6)$$

In the above equations, J_n and Y_n are Bessel functions of the first and second kind, respectively. h_{nm} and k_{nm} are mode consonants of non-axisymmetric mode shape of (n,m), while k_{nm} is related to h_{nm} by $k_{nm}/h_{nm}=\sqrt{2}/(1-\upsilon)$. It should be noted that the relative constants of elastic waves (B_n/A_n, C_n/A_n, B_n/A_n) can be found by solving the equation of det($\mathbf{M}_{4\times4}$) =0. The element of $\mathbf{M}$ was explained in detail in Ref. [8], [14].

In the rest of the paper, the extensional wine glass (2,4) mode ring resonator with the specifications presented in Table 1 has been used to evaluate the frequency response caused by nonlinear effects. Therefore, the subscript nm is omitted and the subscript n=2 representing the second-order mode are used in the following equations. Fig. 2 presents the mode shape and resonance frequency of the extensional wine glass resonator using ANSYS software.

3 Modeling Approach

Since both actuation and capacitive detection of the ring resonator are realized using the inner and outer electrodes, it can be assumed as a two separate ring

resonators attached together at the radius of $(R_i+R_o)/2$ as shown in Fig. 3. Then, each ring resonator is modeled as a distributed element. Considering an infinitesimal element, the gap spacing variations in capacitive transducers are assumed along the radial direction.

Thus, the governing equation of a second-order mechanical system (mass-spring-damper) for an infinitesimal element of the ring resonator can be expressed as:

$$m_o(\theta)x_o'' + b_o(\theta)x_o' + k_{m_o}(\theta)x_o + k_c(x_o - x_i) = 2\left(f_{d_o}(\theta)+f_{s_o}(\theta)\right) \quad (7)$$

$$m_i(\theta)x_i'' + b_i(\theta)x_i' + k_{m_i}(\theta)x_i + k_c(x_i - x_o) = 2\left(f_{d_i}(\theta)+f_{s_i}(\theta)\right) \quad (8)$$

where x represents the radial displacements of the effective lumped mass of m and b, k_m and k_c are damping coefficient, mechanical stiffness and coupling stiffness, respectively. The subscripts i and o denote the inner and outer ring resonators, respectively. The effective masses for infinitesimal element in inner and outer resonators are given by:

$$m_o(\theta) = \frac{\rho t \int_{\frac{R_i+R_o}{2}}^{R_o} U_r^2 r dr}{U_o^2}, m_i(\theta) = \frac{\rho t \int_{R_i}^{\frac{R_i+R_o}{2}} U_r^2 r dr}{U_i^2} \quad (9)$$

Assuming that the first mode is the dominant mode of the system, the inner to outer displacement ratio can be expressed as:

$$\frac{x_i(t,\theta)}{x_o(t,\theta)} \approx \frac{U_i}{U_o} = \gamma \quad (10)$$

Table 1 The related EWG mode parameters for silicon ring resonator.

Parameter	Value	Unit
Inner radius (R_i)	30.16	µm
Outer radius (R_o)	50	µm
Thickness (t)	2	µm
Electrode angle (θ_e)	35	deg
Resonance frequency (f_{nm})	220	MHz
Linear Young's modulus (E_0)	170	GPa
Poisson ratio (υ)	0.28	
Density (ρ)	2330	Kgm^{-3}
First-order corrections (E_1)	-2.6	
Second-order corrections (E_2)	-8.1	

Substituting Eqs. (4) and (10) into Eqs. (7) and (8), and combining them together results in the following expression:

$$\left(m_o(\theta)+m_i(\theta)\cdot\gamma\right)\cos(2\theta)\cdot X_o''(t) + \left(b_o(\theta)+b_i(\theta)\cdot\gamma\right)\cos(2\theta)\cdot X_o'(t) + \left(k_{m_o}(\theta)+k_{m_i}(\theta)\cdot\gamma\right)\cos(2\theta)\cdot X_o(t) = f(\theta) \quad (11)$$

where

$$f(\theta) = 2\left(f_{d_o}(\theta)+f_{d_i}(\theta)\right) + 2\left(f_{s_o}(\theta)+f_{s_i}(\theta)\right) \quad (12)$$

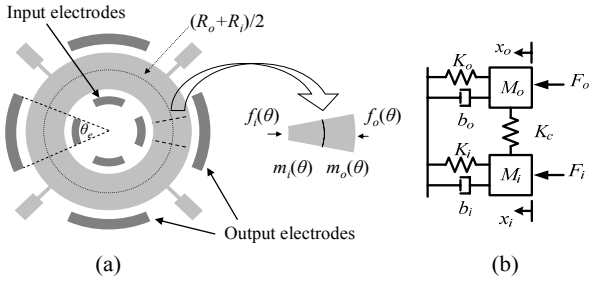

Fig. 3 a) The schematic view of the infinitesimal element b) The equivalent mass-spring-damper system of the ring resonator.

4 Modeling the Origins of the Nonlinearities

Nonlinearities in micromechanical resonators generally arise from electrical and mechanical origins. The electrical nonlinearities include the electrostatic force nonlinearity caused by the variable gap capacitive transducers and the fringing effects. A large structural deformation can be contributed to geometrical and material nonlinearities; classified as mechanical nonlinearities.

4.1 Electrical Nonlinearity

In many micromechanical bulk-mode resonators, the initial gap spacing between electrodes and the resonator is not negligible as compared to the thickness of structure (small aspect ratio) and therefore, the fringing fields are considerable. Hence, the electrostatic force nonlinearity can be modeled using the parallel plate capacitor approximation along with the correction term of C_f representing fringing effects as follows:

$$\left(f_{d_o}(\theta)+f_{d_i}(\theta)\right) = \frac{1}{2}\left(V_P - v_i(t)\right)^2\left(\frac{\partial C_o(\theta)}{\partial x}+\frac{\partial C_i(\theta)}{\partial x}\right)_d \quad (13\text{-a})$$

$$\left(f_{s_o}(\theta)+f_{s_i}(\theta)\right) = \frac{1}{2}V_P^2\left(\frac{\partial C_o(\theta)}{\partial x}+\frac{\partial C_i(\theta)}{\partial x}\right)_s \quad (13\text{-b})$$

where

$$\left(\frac{\partial C_{i,o}(\theta)}{\partial x}\right)_s = \frac{C_f C_{0i,o}(\theta)}{d}\left(\beta + \frac{2}{d}x_{i,o} + \frac{3\beta}{d^2}x_{i,o}^2 + \cdots\right) \quad (14)$$

$$\left(\frac{\partial C_{i,o}(\theta)}{\partial x}\right)_d = \frac{C_f C_{0i,o}(\theta)}{d}\left(1 + \frac{2}{d}x_{i,0} + \frac{3}{d^2}x_{i,o}^2 + \cdots\right) \quad (15)$$

where $C_{0o}(\theta)=\varepsilon R_o t/d$ and $C_{oi}(\theta)=\varepsilon R_i t/d$ imply the capacitance over the outer and inner gaps when the outer and inner radial displacements are equal to zero, and d is the corresponding initial gap spacing. Based on the sense (or drive) electrodes configuration, the value of β would be equal to 1 or -1 as the sense (or drive) electrodes are placed at the same side or opposite side, respectively. The correction term of capacitances for the fringing effects depends on the dimensions of the structure as the following equation [15]:

$$C_f = \begin{cases} 1+4.246\lambda & ; \quad 0<\lambda<0.005 \\ 1+\sqrt{11.0872\lambda^2+0.001097} & ; \quad 0.005<\lambda<0.05 \\ 1+1.9861\lambda^{0.8258} & ; \quad 0.05<\lambda \end{cases} \quad (16)$$

where $\lambda=d/t$ is the initial gap spacing to thickness ratio of the ring structure.

4.2 Mechanical Nonlinearity

Mechanical (material and geometrical) nonlinearities are created by the stresses developing inside the resonator structure under large displacements. Depending on the operation mode, the material or geometrical nonlinearities can be dominant in micromechanical resonators. Unlike the electrical nonlinearities, which can be easily represented by Taylor series with respect to displacement, the mechanical nonlinearities can be approximated by deformation analysis for the bulk-mode ring resonator. For this purpose, the mechanical nonlinearity is first modeled by considering the higher order terms to the mechanical stiffness as follows [10], [16]:

$$k_{m_{i,o}}(\theta) = k_{m_{0i,o}}(\theta)\left(1+k_{1i,o}x_{i,o}+k_{2i,o}x_{i,o}^2\right) \quad (17\text{-a})$$

$$k_{m_{0i,o}}(\theta) = m_{i,o}(\theta)\cdot\omega_{nm}^2 \quad (17\text{-b})$$

In order to consider the geometrical nonlinearities, the geometrical deformation (Fig. 4) caused by large radial displacement in infinitesimal element can be as:

$$A = \int_{\theta_e} A(\theta)\,d\theta \quad (18)$$

$$A(\theta) = R\cdot\theta\cdot t\cdot\left(1-\frac{\Delta R}{R}\right) = A_0(\theta)\left(1-\upsilon\frac{\partial x}{\partial r}\right) \quad (19)$$

Moreover, the large displacement develops internal stresses inside the structure of resonator and therefore, nonlinear elastic behavior of silicon result in nonlinear Young's modulus as follows [10]:

$$E = E_0\left(1+E_1\frac{\partial x}{\partial r}+E_2\left(\frac{\partial x}{\partial r}\right)^2\right) \quad (20)$$

where E_1 and E_2 denote the first-order and second-order corrections to linear Young's modulus of E_0, respectively. The values of E_1 and E_2 are listed in Table 1 for bulk-mode silicon oriented along <100> [16]. Substituting Eqs. (18) and (20) into Eq. (1), multiplying by cos(2θ), and then integrating both sides from θ=0 to 2π results in the approximate expressions for third-order nonlinearity in mechanical stiffness, k_{2o} and k_{2i}, as:

$$k_{2o} = \frac{1}{U_o^2}\frac{\int_{\frac{R_i+R_o}{2}}^{R_o}\Pi(r)dr}{\int_{\frac{R_i+R_o}{2}}^{R_o}\Theta(r)dr} \quad , \quad k_{2i} = \frac{1}{U_i^2}\frac{\int_{R_i}^{\frac{R_i+R_o}{2}}\Pi(r)dr}{\int_{R_i}^{\frac{R_i+R_o}{2}}\Theta(r)dr} \quad (21)$$

$$\Pi(r) = U_r\left[\left(E_2(2\upsilon-3)+E_1\upsilon\right)\frac{U_r}{r}\left(\frac{\partial U_r}{\partial r}\right)^2 + (E_2-E_1\upsilon)\left(\left(\frac{\partial U_r}{\partial r}\right)^2\left(\frac{\partial^2 U_r}{\partial r^2}\right)r+\left(\frac{\partial U_r}{\partial r}\right)^3\right)\right] \quad (22)$$

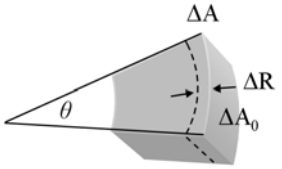

Fig. 4 The geometrical variation in infinitesimal element of the ring resonator.

$$\Theta(r) = U_r\left(\left(\frac{\partial^2 U_r}{\partial r^2}\right)r+\left(\frac{\partial U_r}{\partial r}\right)+(2\upsilon-3)\frac{U_r}{r}\right) \quad (23)$$

In fact, the second-order nonlinearity term caused by symmetric structure of the ring and mode shape is omitted. Using the self-written numerical codes in MATLAB software, the values of k_{2o} and k_{2i} for the case study of this paper were calculated to be -2.842×10^{-11} Nm^{-1} and -1.024×10^{-10} Nm^{-1}, respectively.

5 Analysis of the Nonlinear Effects

Based on the electrostatic and mechanical nonlinearities and multiplying Eq. (11) by cos(2θ) and then integrating over the range of 0 to 2π, the governing equation of a second-order mechanical system of the micromechanical ring can be rewritten as:

$$X_o''(t)+\frac{\omega_t}{Q}\cdot X_o'(t)+\omega_t^2\cdot X_o(t)+\Omega_2X_o^2(t) + \Omega_3X_o^3(t) = g_0+v_i(t)\left(g_1+g_2X_o(t)+g_3X_o^2(t)\right) \quad (24)$$

The notations used in the above equation are presented in Table 2.

Eq. (24) is called Duffing's equation, where ω_t, Q and θ_e are the resonance frequency caused by electrical nonlinearity, mechanical quality factor and electrode-to-resonator overlap angle, respectively. The DC term in Eq. (24) has no effect on the nonlinear analysis of the frequency response and it can be ignored as follows:

$$X_o''(t)+\frac{\omega_t}{Q}\cdot X_o'(t)+\omega_t^2\cdot X_o(t) = \alpha_0 + d\left(\alpha_1X_o(t)+\alpha_2X_o^2(t)+\alpha_3X_o^3(t)\right) \quad (25)$$

where

$$\alpha_0 = g_1v_i(t), \qquad \alpha_1 = \frac{g_2v_i(t)}{d}$$
$$\alpha_2 = \frac{\left(g_3v_i(t)-\Omega_2\right)}{d}, \qquad \alpha_3 = \frac{-\Omega_3}{d} \quad (26)$$

The approximate analytic method can be used to solve the Eq. (25). Assuming weak nonlinearities, this problem can be solved by perturbation technique. This method assumes that the resonance frequency along with the solution varies as a function of perturbation terms and the solution is given by:

$$X_o(t) = X_{o_0}(t)+\sum_{n=1}^{\infty}d^nX_{o_n}(t) \quad (27)$$

Table 2 Definitions used in the Eq. (24).

	Definition
ω_t	$\sqrt{\left(K_{m_0}-k_e\right)M^{-1}}=\sqrt{K_{re}M^{-1}}$
K_{m_0}	$\pi\left(K_{m_{0o}}+\gamma K_{m_{0i}}\right)$
K_e	$V_P^2 d^{-2}\left(\left(\gamma C_{0i}-C_{0o}\right)\left(\sin(2\theta_e)+2\theta_e\right)\right)$
$K_{m_{0o,i}}$	$\int_0^{2\pi} k_{m_{0o,i}}(\theta)\cdot\cos^2(2\theta)d\theta$
Q	$B^{-1}\sqrt{MK_{re}}$
B	$\int_0^{2\pi}\left(b_o(\theta)+b_i(\theta)\cdot\gamma\right)\cdot\cos^2(2\theta)d\theta$
g_0	$V_P^2 d^{-1}M^{-1}\left(\beta+1\right)\left(C_{0i}-C_{0o}\right)\sin(\theta_e)$
g_1	$-2V_P d^{-1}M^{-1}\left(C_{0i}-C_{0o}\right)\sin(\theta_e)$
g_2	$-V_P d^{-2}M^{-1}\left(\gamma C_{0i}-C_{0o}\right)\left(\sin(2\theta_e)+2\theta_e\right)$
g_3	$-2V_P d^{-3}M^{-1}\left(\gamma^2 C_{0i}-C_{0o}\right)\left(\cos^2(\theta_e)+2\right)\sin(\theta_e)$
Ω_2	$-V_P^2 d^{-3}M^{-1}\left(\beta+1\right)\left(\gamma^2 C_{0i}-C_{0o}\right)\times$ $\left(\cos^2(\theta_e)+2\right)\sin(\theta_e)$
Ω_3	$\frac{3\pi}{4}M^{-1}\left(K_{m_{0o}}k_{2o}+\gamma^3 K_{m_{0i}}k_{2i}\right)-V_P^2 d^{-4}\times$ $\left(\gamma^3 C_{0i}-C_{0o}\right)\left(\sin(2\theta_e)\left(\frac{1}{3}\cos(\theta_e)+\frac{1}{2}\right)+\theta_e\right)$

$$\omega_t' = \omega_t + \sum_{n=1}^{\infty} d^n \omega_n \tag{28}$$

The second order approximation of this solution can be used to achieve a more exact evaluation as:

$$X_o(t) = X_{o_0}(t) + dX_{o_1}(t) \tag{29}$$

$$\omega_t' = \omega_t + d\,\omega_1 \tag{30}$$

Substituting Eqs. (29) and (30) into Eq. (25) and grouping the terms in power of d, the two following expressions are obtained:

$$X_{o_0}''(t) + \frac{\omega_t'}{Q}X_{o_0}'(t) + \omega_t'^2 X_{o_0}(t) = \alpha_0 \tag{31}$$

$$X_{o_1}''(t) + \frac{\omega_t'}{Q}\cdot X_{o_1}'(t) + \omega_t'^2\cdot X_{o_1}(t) = \frac{\omega_1}{Q}\cdot X_{o_0}'(t) + \left(2\omega_t'\omega_1+\alpha_1\right)X_{o_0}(t) + \alpha_2 X_{o_0}^2(t) + \alpha_3 X_{o_0}^3(t) \tag{32}$$

When the AC-drive voltage of $v_i(t)=|v_i|\cos(\omega t)$ is applied, the solution of $X_{o0}(t)$ would be as:

$$X_{o_0}(t) = \mathrm{Re}\left(g_1|v_i|\mathrm{e}^{\mathrm{j}\omega t}\cdot H(\omega)\right) = g_1|v_i|\left(H'_\omega\cos(\omega t) - H''_\omega\sin(\omega t)\right) \tag{33}$$

where

$$H(\omega) = \frac{1}{\omega_t'^2-\omega^2+\mathrm{j}\frac{\omega\omega_t'}{Q}} = H'_\omega + \mathrm{j}H''_\omega \tag{34}$$

where H'_ω and H''_ω denote the real and imaginary parts of the transfer function of $H(\omega)$, respectively. Substituting Eq. (33) into the right hand side of Eq. (32) and setting the secular terms to zero, the expression of ω_1 is approximately given by:

$$\omega_1 = -\frac{3}{8}\frac{\alpha_3 g_1^2|v_i|^2\left(H'^2_\omega + H''^2_\omega\right)}{\omega_t'} \tag{35}$$

Thus, by substituting Eq. (35) into (30), the resonance frequency caused by mechanical and electrical nonlinearities, $\acute{\omega}_t$, is expressed as follows:

$$\omega_t' = \frac{\omega_t}{2} + \frac{1}{2}\sqrt{\omega_t^2 + \frac{3}{2}\Omega_3 g_1^2 v_i^2\left(H'^2_\omega + H''^2_\omega\right)} \tag{36}$$

As shown in the Eq. (36), $\acute{\omega}_t$ is a function of the amplitude of the first-order approximation of the solution. By Substituting Eq. (33) into (32), the solution of $X_{o1}(t)$ is calculated and, therefore, $X_o(t)$ can be expressed as follows:

$$X_o(t) = g_1|v_i|\left(\left[G_1'\cos(\omega t) - G_1''\sin(\omega t)\right] + \left[G_2'\cos(2\omega t) - G_2''\sin(2\omega t)\right] + \left[G_3'\cos(3\omega t) - G_3''\sin(3\omega t)\right]\right) \tag{37}$$

where

$$G_1' = \frac{3}{4}g_1^2|v_i|^2\Omega_3 H''^4_\omega \tag{38-a}$$

$$G_1'' = H''_\omega\left(1+\frac{1}{4}g_1 g_3|v_i|^2 H''^2_\omega\right) \tag{38-b}$$

$$G_2' = -\frac{1}{2}|v_i|H''_\omega\left(g_2 H''_{2\omega} - g_1\Omega_2 H''_\omega H'_{2\omega}\right) \tag{39-a}$$

$$G_2'' = \frac{1}{2}|v_i|H''_\omega\left(g_1\Omega_2 H''_\omega H''_{2\omega} + g_2 H'_{2\omega}\right) \tag{39-b}$$

$$G_3' = -\frac{1}{4}g_1|v_i|^2 H''^2_\omega\left(g_1\Omega_3 H''_{3\omega}H''_\omega + g_3 H'_{3\omega}\right) \tag{40-a}$$

$$G_3'' = -\frac{1}{4}g_1|v_i|^2 H''^2_\omega\left(\frac{1}{2}g_1\Omega_3 H'_{3\omega}H''_\omega + g_3 H''_{3\omega}\right) \tag{40-b}$$

where $H'_{n\omega}$ and $H''_{n\omega}$ (n= 2,3), denote the real and imaginary parts of the transfer function of $H(n\omega)$, respectively. Substituting Eq. (37) into (5), the output current for infinitesimal element of micromechanical ring resonator can be expressed using the following equation as:

$$i_{om}(t,\theta) = \frac{2V_P}{d^3}\frac{\partial x_o(t,\theta)}{\partial t}\left[d^2\beta\left(C_{0o}(\theta)+\gamma C_{0i}(\theta)\right) + 2d\left(C_{0o}+\gamma^2 C_{0i}\right)x_o(t,\theta) + 3\beta\left(C_{0o}+\gamma^3 C_{0i}\right)x_o^2(t,\theta)\right] \tag{41}$$

Multiplying by cos(2θ) and then integrating both sides, from 0 to 2π, the total output current due to the AC-drive voltage at the resonance frequency is finally derived as:

$$i_o(t)=\sum_{q=1}^{\infty}\left|i_{oq}\right|\cos(q\omega t+\psi_q) \quad (42)$$

The experimental results of the study conducted by Xie *et al*. [8] were used to experimentally verify derived expression for presented model in linear regime and electrical stiffness. As shown in Fig. 5(a) and 5(b), the frequency response is measured using the mixing approach [8]. To adapt this approach to the proposed model, the equations of $|v_i|=(v_{LO}|v_{RF}|)/2$ and $P_o=(R_L|i_o|^2)/2$, (R_L=50 Ω) [17] are used in the derived expressions.

It can be seen from Figs. 5 and 6(a) that the frequency response and resonance frequency change of the nonlinear model agree well with experimental data. However, the low difference between their amplitude and resonance frequency may be due to the parasitic capacitance and resistance in experimental measurements. According to the expression of electrical stiffness, K_e, when DC-bias voltage (V_P), increases or the initial gap spacing between the electrodes to resonator (d) decreases, the resonance frequency caused by electrical nonlinearity (ω_t), shifts down as shown in Fig. 6(b). In order to address the nonlinear effects on the frequency response, assuming that the first mode is the dominant mode and using the first-order approximation, the solution is assumed as follows:

$$X_o(t)=X_o\cos(\omega t) \quad (43)$$

$$X_o=g_1\left|v_i\right|\sqrt{H_\omega'^2+H_\omega''^2} \quad (44)$$

Thus, the phase difference between the AC-drive voltage $v_i(t)$, and solution $X_o(t)$, is maintained as the phase of applied voltage and is fixed as the phase of solution as follows:

$$v_i(t)=\left|v_i\right|\cos(\omega t-\varphi)=v_1\cos(\omega t)+v_2\sin(\omega t) \quad (45)$$

Substituting Eqs. (28) and (29) into (25) and using the method of harmonic balance, the following equations are obtained:

$$v_1=\frac{X_o\left(3\Omega_3X_o^2+4\left(\omega^2-\omega_t^2\right)\right)}{3g_3X_o^2+4g_1},\quad v_2=\frac{4\omega_t\omega X_o}{Q\left(g_3X_{o0}^2+4g_1\right)} \quad (46)$$

Substituting Eq. (46) into $v_1^2+v_2^2=v_i^2$, leads to the relation between the amplitude of AC-drive voltage and vibration amplitude as:

$$\left(\frac{X_o\left(3\Omega_3X_o^2+4\left(\omega^2-\omega_t^2\right)\right)}{3g_3X_o^2+4g_1}\right)^2+\left(\frac{4\omega_t\omega X_o}{Q\left(g_3X_o^2+4g_1\right)}\right)^2=\left|v_i\right|^2 \quad (47)$$

To study the effects of drive voltage on the frequency response, the DC-bias voltage V_P, is assumed

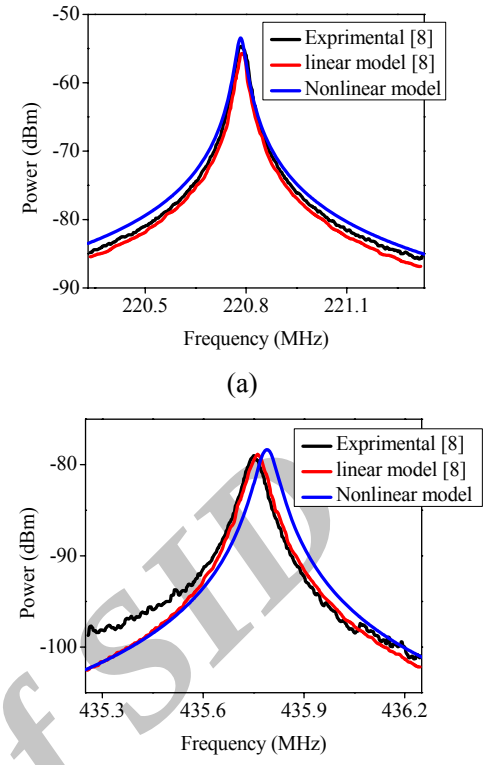

Fig. 5 The frequency response for polysilicon EWG mode ring resonators a) 220.8 MHz b) 435.8 MHz.

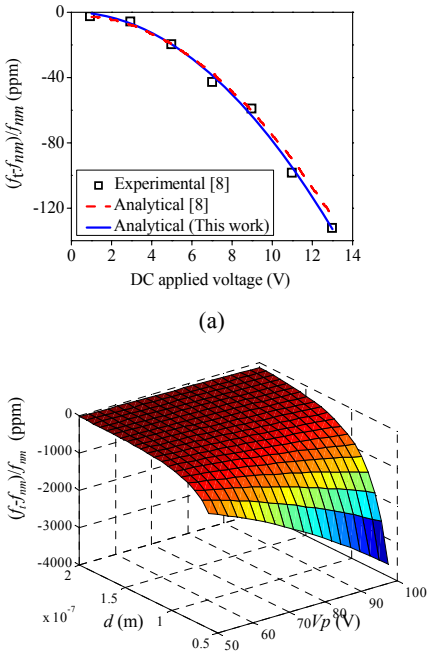

Fig. 6 The fractional resonance frequency change caused by electrical nonlinearity for a) Polysilicon EWG ring resonator with f_0=220.8 MHz b) Silicon EWG mode ring resonator (as Table 1)

constant and the drive voltage varies. In Fig. 7(a), it is shown that as drive voltage (v_i) increases, the resonator frequency response changes from an almost linear curve to a completely nonlinear one (hysteresis). In fact, higher drive voltage leads to larger vibrations and eventually results in a jump in frequency response. This behavior is evident when there are two amplitudes of vibration for a given forcing frequency at high drive voltage. Moreover, the peak frequency tilts to a lower frequency as the vibration amplitude increases and the ring resonator, therefore, exhibits a softening behavior.

It can also be seen from Fig. 8 that an increase of the V_P or a decrease in d, tilts the resonance peak more, and the softening behavior of the micromechanical ring resonator becomes more pronounced. Quality factor is a fundamental parameter to design of micromechanical resonators for MEMS-based filters with a low insertion loss. There exist several intrinsic and extrinsic energy-loss mechanisms in the bulk-mode resonators like air damping, anchor loss and thermoelastic damping (TED); for a bulk-mode resonator operating in high vacuum, the air damping mechanism can be ignored. Also, in these resonators, the thermoelastic damping is negligible as compared to the anchor loss and therefore, anchor loss is the dominant energy-loss mechanism [18]. It is demonstrated that, anchor loss is strongly dependent on the support beam dimensions, and it can be reduced by mechanically isolating the support beams from the substrate and optimum designing of their dimensions [19], [20]. As shown in Fig. 9(a), the nonlinear effects on frequency response become more apparent by increasing quality factor.

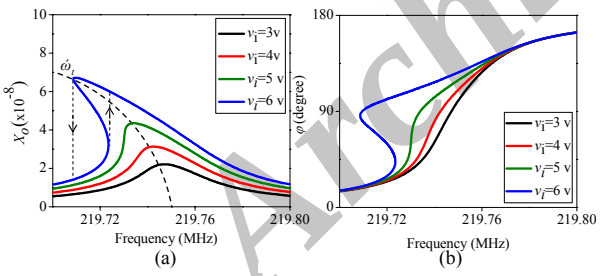

Fig. 7 The effect of AC-drive voltage on frequency response for EWG ring resonator with Q=8000, d=90 nm , V_P=100 V.

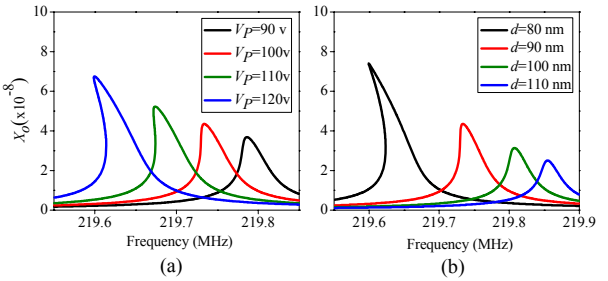

Fig. 8 The effects of DC-bias voltage and initial gap spacing variations on frequency response for EWG ring resonator with Q=8000 a) d=90 nm and v_i=5 VPP b) V_P=100 V and v_i=5 V_{PP}.

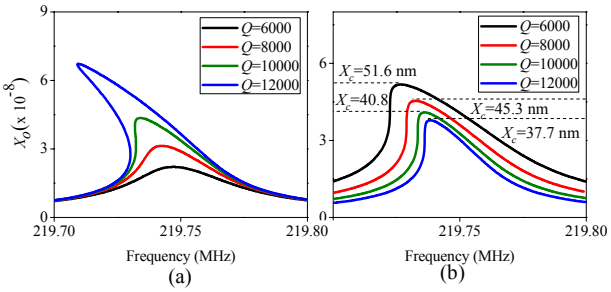

Fig. 9 The effect of Q-factor on a) Frequency response for EWG ring resonator with v_i=4 V_{PP}, d=90 nm and V_P=100 V b) Critical vibration amplitude (X_C) of a EWG ring resonator with d=90 nm and V_P=100 V.

The greatest vibration amplitude before hysteresis, called the critical vibration amplitude, X_c, can be used to estimate the limit for power handling as given by $E_c=(K_{m0}X_c^2)/2$ [10]. Where E_c is the maximum stable energy stored in the resonator. In Fig. 9(b), it is shown that under the same conditions, a higher quality factor decreases the critical vibration amplitude and therefore, lowers maximum stable energy stored.

To verify the presented model, the results of nonlinear behavior of the ring resonator were compared with two analytical models. Zhang *et al.* [9] used a method of two-variable expansion to analyze the Duffing's equation when the driving frequency is close to the resonance frequency of ω_t. Moreover, they proposed an effective third-order stiffness (K_{2eff}) as a nonlinear parameter, which the transition of this parameter from positive to negative will change the left hand side bifurcation to right hand side bifurcation of the resonator frequency response. According to the two-variable expansion method, the effective third-order stiffness was obtained for micromechanical ring resonator as follows:

$$K_{2eff} = \frac{(\Lambda_m + \Lambda_e)}{\left((\gamma C_{0i} - C_{0o})(\sin(2\theta_e) + 2\theta_e)\right)} \tag{48}$$

where

$$\Lambda_m = \frac{3}{2}\pi\left(K_{m_{0o}}k_{2o} + \gamma^3 K_{m_{0i}}k_{2i}\right)d^2V_P^{-2} \tag{49}$$

$$\Lambda_e = \left(\gamma^3 C_{0i} - C_{0o}\right)(1+\frac{2}{3}\cos(2\zeta))d^{-2}\times \left[\sin(2\theta_e)\left(2\cos(\theta_e)+3\right)+6\theta_e\right] \tag{50}$$

where, ξ can be calculated by numerically solution of Eqs. (51) and (52):

$$\sin(2\xi) = \frac{-4\omega_t}{Q\left(4d - g_3|v_i|\Theta\right)} \tag{51}$$

$$\Theta = \frac{-4d\left(1+\cos(2\xi)\right)}{3\Omega_3 - 2g_3|v_i|\cos(2\xi)} \tag{52}$$

As shown in Eq. (48), Λ_m and Λ_e denote the nonlinear parameters due to third-order mechanical and electrical nonlinearity respectively. From Fig. 10, it is

found that, the sign of K_{2eff} is fixed for different value of DC-bias voltage. This is different from flexural-mode resonators, where exhibit hardening behavior and the sign of K_{2eff} can be changed with DC-bias voltage.

Kaajakari *et al*. [10], [11] used a method of successive approximations to obtain a solution to Duffing's equation assuming the micromechanical resonator with high quality factor. However, some effects of electrostatic force on Duffing's equation were not taken into account.

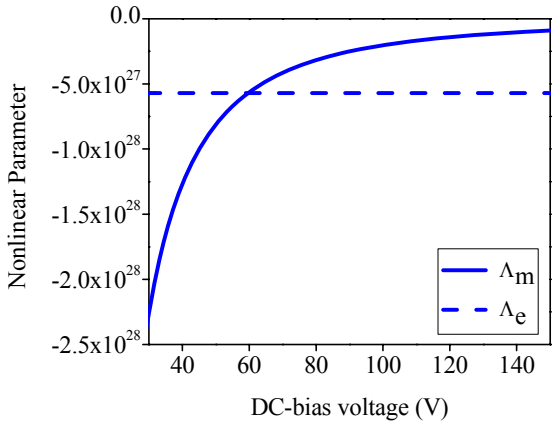

Fig. 10 The nonlinear parameters versus DC-bias voltage for EWG ring resonator with Q=8000, d=90 nm and v_i=5 V_{PP}.

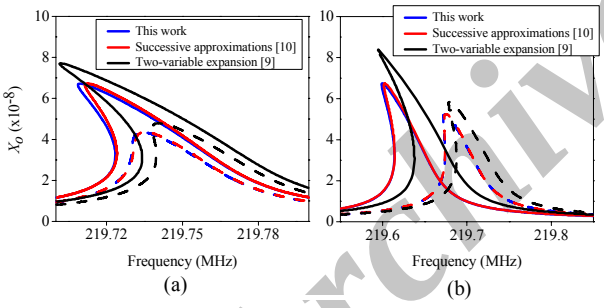

Fig. 11 The comparison between the result of analytical methods for EWG ring resonator with Q=8000, d=90 nm a) v_i=5 VPP (dash line) and v_i=6 V_{PP} (solid line) with V_P=100 V b) V_P=110 V (dash line), V_P=120 V (solid line) with v_i=5 V_{PP}.

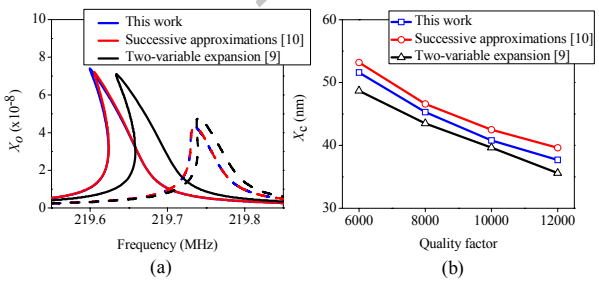

Fig. 12 The comparison between the result of analytical methods for EWG ring resonator with V_P=100 V a) Effect of initial gap spacing, d=90 nm (dash line) and d=80 nm (solid line) with Q=8000 and v_i=5 V_{PP} b) Effects of quality factor with d=90 nm.

As shown in Figs. 11 and 12, the analytical results of the paper are in good agreement with the results from successive approximations method. However, in two-variable expansion method, the resonance frequency shifts down less than other methods with increasing DC-bias voltage and decreasing initial gap spacing. Moreover, the results from the analytical models indicate that the ring resonator exhibit softening behavior in nonlinear regime.

6 Conclusion

This paper deals with the nonlinear modeling of silicon micromechanical ring resonators with electrostatic actuation and detection on both inner and outer radius. The origins of nonlinearities in the micromechanical resonators were completely modeled as a distributed element using Taylor series and deformation analysis. Based on the derived expressions for third-order nonlinearities in mechanical and electrical stiffness, the expression of the resonance frequency was obtained using the perturbation method. The nonlinear effects on frequency response were addressed in details and the results of the paper were compared with two analytical models, as well. It was shown that the micromechanical ring resonator exhibits the softening behavior. Moreover, there is a trade-off between the conventional methods to reduce motional resistance and stability of the frequency response in micromechanical ring resonators. While the DC-bias voltage is increased or the initial gap spacing is decreased, the ring resonator becomes more susceptible to nonlinear effects. In addition, increasing the resonator quality factor was shown to tilt the peak frequency toward lower frequencies and decrease the maximum energy stored. The presented model and the results of this paper allow designers to optimize the design of micromechanical ring resonators and improve the performance of MEMS-based filters and oscillators.

References

[1] Fathipour M., Refan M. H. and Ebrahimi S. M., "Design of a resonant suspended gate MOSFET with retrograde channel doping", *Iranian Journal of Electrical & Electronic Engineering*, Vol. 6, No. 2, pp. 77-83, June 2010.

[2] Mestrom R. M. C., Fey R. H. B. and Nijmeijer H., "Phase feedback for nonlinear MEM resonators in oscillator circuits", *IEEE/ASME Transactions on Mechartonics*, Vol. 14, No. 4, pp. 423-433, Aug. 2009.

[3] Demirci M. U., Ahdelmoneum M. A. and Nguyen C. T. C., "Mechanically corner-coupled square microresonator array for reduced series motional resistance", *Journal of Microelectromechanical Systems*, Vol. 15, No. 6, pp. 1419-1436, Dec. 2006.

[4] Mestrom R. M. C., Fey R. H. B., Van Beekb J. T. M., Phanb K. L. and Nijmeijer H., "Modelling the

dynamics of a MEMS resonator: Simulations and experiments", *Sensors & Actuators A: Physical*, Vol. 142, pp. 306-315, Apr. 2007.
[5] Gui C., Legtenberg R., Tilmans H. A. C., Fluitman J. H. J. and Elwenspoek M., "Nonlinearity and hysteresis of resonant strain gauges", *Journal of Microelectromechanical Systems*, Vol. 7, No. 1, , pp. 122-127, Mar. 1998.
[6] Alastalo A. T. and Kaajakari V., "Third-order intermodulation in microelectromechanical filters coupled with capacitive transducers", *Journal of Microelectromechanical Systems*, Vol. 15, No. 1, pp. 141-148, Feb. 2006.
[7] Shao L. C., Niu T. and Palaniapan M., "Nonlinearities in a high-Q SOI Lame-mode bulk resonator", *Journal of Micromechanics and Microengineering*, Vol. 19, pp. 1-8, Jun. 2009.
[8] Xie Y., Li S. S., Lin Y. W., Ren Z. and Nguyen C. T. C., "1.52-GHz micromechanical extensional wine-glass mode ring resonators", *IEEE Transaction on Ultrasonics, Ferroelectrics, and Frequency Control*, Vol. 55, No. 4, pp. 890-907, Apr. 2008.
[9] Zhang W., Baskaran R. and Turner K. L., "Effect of cubic nonlinearity on auto-parametrically amplified resonant MEMS mass sensor", *Sensors & Actuators A: Physical*, Vol. 102, pp. 139-150, Aug. 2002.
[10] Kaajakari V., Mattila T., Lipsanen A. and Oja A., "Nonlinear mechanical effects in silicon longitudinal mode beam resonators", *Sensors & Actuators A: Physical*, Vol. 120, pp. 64-70, Dec. 2004.
[11] Kaajakari V., Mattila T., Kiihamaki J., Kattelus H., Oja A. and Seppa H. "Nonlinearities in single-crystal silicon micromechanical resonators", *The International IEEE Conference on Solid state Sensors, Actuators and Microsystem*, pp. 1574-1577, 2003.
[12] Hao Z., Pourkamali S. and Farrokh Ayazi., "VHF Single-Crystal Silicon Elliptic Bulk-Mode Capacitive Disk Resonators-Part I: Design and Modeling", *Journal of Microelectromechanical Systems*, Vol. 13, No. 6, pp. 141-148, Dec. 2004.
[13] Sadd M. H., *Elasticity - Theory, Applications, and Numerics*, 2nd Edition, Burlington, Academic Press, 2009.
[14] Takano T., Hirata H. and Tomikawa Y., "Analysis of non-axisymmetric vibration mode piezoelectric annular plate and its application to an ultrasonic motor", *IEEE Transaction on Ultrasonics, Ferroelectrics, and Frequency Control*, Vol. 37, No. 4, pp. 558-565, Nov. 1990.
[15] Marques F., Castello R. C. and Shkel A. M., "Modelling the electrostatic actuation of MEMS: state of the art", *IOC-DT-P*, Vol. 18, pp. 1-33, Sep. 2005.
[16] Kaajakari V., Mattila T., Lipsanen A., Oja A. and Seppa H., "Nonlinear limits for single-crystal silicon microresonators", *Journal of Microelectromechanical Systems*, Vol. 13, No. 5, pp. 715-724, Oct. 2004.
[17] Wang, J., Ren, Z. and Nguyen, C. T. C., "1.156-GHz Self-Aligned vibrating micromechanical disk resonator", *IEEE Transaction on Ultrasonics, Ferroelectrics, and Frequency Control*, Vol. 51, No. 12, pp. 890-907, Dec. 2004.
[18] Hao, Z. and Ayazi, F., "Support loss in micromechanical disk resonators", *The International IEEE Conference on Micro Electro Mechanical Systems*, pp. 137–141, 2005.
[19] Lee J., Yan J. and Seshia A. A., "Study of lateral mode SOI-MEMS resonators for reduced anchor loss", *Journal of Micromechanics and Microengineering*, Vol. 21, pp. 1-10, Mar. 2011.
[20] Khine L. and Palaniapan M., "High-Q bulk-mode SOI square resonators with straight beam anchors", *Journal of Micromechanics and Microengineering*, Vol. 19, pp. 1-10, Jan. 2009.

Abolfazl Bijari was born in Birjand, Iran in 1982. He received B.S. degree in telecommunication engineering and M.S. in electronic engineering from Ferdowsi University of Mashhad (FUM), Iran in 2005 and 2007, respectively. He is currently PhD candidate in electronic engineering at the Department of Electrical Engineering, Faculty of Engineering, Ferdowsi University of Mashhad. His research interests include micromechanical resonators, filters and nonlinear effect on MEMS-based devices. He also took part in a year joint collaboration at the Synchrotron Light Research Institution (SLRI), Nakhon Ratchasima, Thailand in 2011 where he worked on LIGA-based micromechanical resonators.

Sayyed-Hossein Keshmiri received his B.Sc. degree in Physics from Mashhad University in 1969, M.Tech. from Brunel University (London, UK) in 1971, and Ph.D. degree from The Pennsylvania State University (University Park, USA) in 1981. He started work in Ferdowsi University of Mashhad in 1971 first in Physics Department, and later was transferred to the Electrical Engineering Department. He is currently a professor of Electrical Engineering. His research interests include design and fabrication of photovoltaic solar cells, MEMS devices, transparent-conducting (TC) films, structural-defect passivation in silicon and in TC films, multilayer thin-film optical filters, and thin-film gas sensors.

Winai Wanburee was born in Roi-et, Thailand in 1982. He received the B.S. and M.S. degrees in the electrical engineering from Suranaree University of Technology (SUT), Nakhon Ratchasima, Thailand in 2005 and 2007, respectively. He has been with Synchrotron Light Research Institute (SLRI), Nakhon ratchasima, Thailand as a member of Research Staff in SUT-MEMS Laboratory Since 2005. He is currently working toward the Ph.D. degree at Suranaree University of Technology since 2007. His research interests include design, analysis of micro-devices such as comb-drive actuator and RF switch, and development of X-ray lithography process.